MEASUREMENTS OF HYDRATE FORMATION IN SANDSTONE

J.C. Stevens[1], B.A. Baldwin[2], A. Graue[3], G. Ersland[3], J. Husebø[3], and J.J. Howard[1]
[1]ConocoPhillips [2]Green Country Petrophysics, LLC [3]University of Bergen

This paper was prepared for presentation at the International Symposium of the Society of Core Analysts held in Calgary, Canada, 10-12 September, 2007

ABSTRACT

Methane and carbon dioxide hydrates were formed in sandstone samples for a series of laboratory experiments to evaluate gas production scenarios from natural gas hydrates. Methods were developed that yield rapid and complete conversion of the water and gas mixtures in the pores into a solid hydrate phase. Hydrates were formed under a range of conditions including initial water and gas saturations, water composition, and temperature. The sandstone is from the Bentheim formation and is characterized by a quartz-rich framework with small amounts of clay in pores that average 125 microns in diameter. The sandstone samples were placed in a pressurized sample holder that was suitable for MRI imaging. Sample confining pressure was maintained with cooled Fluorinert run through a home-built heat-exchanger that effectively controlled the sample temperature to within 0.1^{o}C over several months for a given experiment. Methane and carbon dioxide hydrates were formed at ~4^{o}C and 8.3 MPa gas pressure. Hydrate formation was monitored with a combination of MRI images, permeability measurements and pressure-volume data from the pumps that control gas and water supply to the sample. Hydrate formation rates and patterns were extracted from these various data sources and were used in larger-scale simulations of hydrate behavior in reservoirs. The ease and reproducibility of hydrate formation allows for investigations into the hydrate rock physics problem of how to characterize the distribution of hydrates in pores.

INTRODUCTION

Interest in natural gas hydrates as a potential energy resource has grown significantly in recent years as awareness of the volumes of recoverable gas becomes more focused (Sloan, 1998). While there are tremendous volumes of gas in hydrates associated with fine-grain sediments in deep marine environments that defy current techniques for commercial production, there remain significant volumes of gas-bearing hydrates in northern regions associated with permafrost environments that may lend themselves to successful recovery of natural gas. Several of the critical issues include the range of hydrate saturation in these coarser-grain sediments, the habit of hydrate growth within pores and how it affects permeability to gas. The evaluation of potential production scenarios also requires knowledge of the recovery efficiency of the natural gas from the hydrate and the corresponding amounts of produced water.

Since the opportunities to test the producibility of hydrate reservoirs to date are very limited, the efforts to acquire the necessary reservoir engineering data needed for planning purposes has focused on laboratory tests. Actual core samples from hydrate deposits are rare and often corrupted by the coring procedure where natural gas is released from the hydrate as the core is depressurized on its way to the surface. New pressurized coring devices are currently being developed in order to improve the recovery of hydrate-saturated core samples. This leaves efforts to form natural gas hydrates in a laboratory setting as the best means available to study potential production scenarios.

A number of recent studies have reported the successful formation of natural gas hydrates, predominantly methane, in various porous media. While a number of theoretical studies focused on hydrate formation in very fine-grain pores, i.e. nano-scale features, and the relationship with temperature depression as observed with ice in very small pores. In contrast, the laboratory studies on hydrate formation have emphasized pore systems with much larger pores where the P-T stability relationships for various hydrate-water-gas combinations as developed for bulk hydrate experiments should remain valid.

Porous media for these laboratory efforts range from packings of well-sorted sand grains to actual sandstones. Common to both is that the systems are very simple in terms of lithology; quartz-rich with minimal clay minerals. The laboratory hydrates are formed with a variety of gases; methane, carbon dioxide and Tetrahydrofluran (THF) are the most common (Buffett and Zatsepina, 2000; Hetland and Bratteli, 2005; Baldwin et al., 2003). THF hydrates have the advantage in that they form at atmospheric pressure and near-zero temperatures, whilst methane and carbon dioxide hydrates require significant pore pressure in addition to the reduced temperatures to form. These experiments vary in the amounts of water and gas emplaced in the pores and whether the system includes excess free gas or is gas starved.

The experiments reported in this study are unique in that methane hydrate formation is monitored with Magnetic Resonance Imager, MRI, images along with the more traditional pressure and volume changes associated with gas consumption during hydrate formation. The advantage provided by a MRI experiment is that the images are sensitive to the presence of free methane gas and free water in the pores, but they do not respond to the presence of hydrogen in a solid phase such as ice or hydrate (Moudrakovski et al., 2004). The hydrogen in the hydrate cage structure and the clathrated gas molecules have very fast relaxation rates that cannot be detected by standard imaging sequences. This simple on-off relationship between free methane and water versus hydrate makes for easily discernible measurements of hydrate formation progress and stability during other tests.

PROCEDURES

Hydrates were formed in the pore space of a high porosity, high permeability sandstone acquired from the Bentheim quarry in Lower Saxony, Germany. The Bentheim sample used in these experiments had a porosity of 23% and a permeability of 1100 mD and was

characterized by a uniform pore geometry with an average pore diameter of 125 microns. Two core plug geometries were used in these experiments. The first was a standard cylindrical plug, 3.75 cm diameter and varying lengths between 4 and 6 cm. The second arrangement split an original cylinder down the long axis of the plug and inserted a 4 mm thick acetal polyoxymethylene, POM, spacer between the two halves. The arrangement of core halves and spacer required careful milling in a machine shop. This ensured that the completed assembly maintained a true cylindrical shape for use in the sample holder. The spacer had a known volume of free space and small openings in the supporting frame such that fluids could easily enter and leave the spacer. The purpose of the spacer was to simulate a fracture opening in the sample where fluids had enhanced access to the porous media. The spacer also proved to be an effective region for the accumulation of produced gas from the hydrates.

The cylindrical core plug or plug halves plus spacer assembly was encased in shrink tubing before placement in the sleeve of the sample holder. The shrink tubing isolated the core plug from the confining fluid. The sample holder was designed for use in a Magnetic Resonance Imager, MRI, and was constructed of low-inductance fiberglass and titanium end pieces that minimized the loss of RF signal in the MRI experiments. The end pieces had multiple ports for fluids and temperature sensors. Confining pressure was applied though circulating Fluorinert™ through the sample holder. A liner composed of Aflas® prevented the loss of Fluorinert through the walls of the fiberglass housing.

The Fluorinert was cooled in a bath located several meters from the sample holder and the MRI. This allowed for the Fluorinert to cool the sample holder to near-freezing temperatures while also serving it main purpose of applying the confining pressure. The flow line from the pump controlling Fluorinert pressure was cooled both at the source and with a novel heat-exchange technique. The stainless steel $1/4^{th}$ inch line for the Fluorinert circulation was encased in a larger PVC line that circulated a non-toxic propylene glycol / water mixture. It was possible to maintain temperature stability of $0.1^{o}C$ for months at a time.

The introduction of fluids to the core sample was controlled by a series of pumps connected to the inlet ports on the sample holder's end pieces. Flow rates, pressures and volumes of water, nitrogen, and methane gas were controlled by these pumps.

The core plugs were partially saturated with water in one of two methods. The first involved setting the saturation between 20 and 100% before the sample holder was assembled. The second method assembled the dry core in the holder first and then a known volume of water was introduced through the spacer. Imbibition produced a near uniform distribution of the water in the core plug. The distribution of the water was measured by MRI scans prior to starting the hydrate formation experiment. Sometimes the process of core assembly and water introduction was repeated several times until a uniform saturation distribution was obtained. Water salinity varied from 0.1 to 5.0 weight percent NaCl although most of the experiments were run with salinities in the range of

0.1 and 3.0 weight percent that corresponded to values anticipated in permafrost-related hydrate deposits (Sloan, 1997). The presence of salt, which acts as a hydrate formation inhibitor, ensured that not all of the water was transformed into hydrate.

Methane gas was added to the water-saturated core plug through the inlet lines at a pore pressure of 8.3 MPa (1200 psi). The methane pressure in the system was kept constant with a Quizix pump so that any pressure reduction associated with methane consumption during hydrate formation was compensated by a measurable methane volume increase that maintained the system's constant pressure. The sequence of introducing methane and water was switched on several experiments where the pores were initially saturated with methane at a pore pressure of 8.3 MPa before the water volume was added.

The core plug assembly was cooled to 3 to 4^{o}C through the circulation of the chilled Fluorinert through the sample holder. This process generally required 2 to 6 hours to drop from room temperature to the experimental run temperature. Once at the desired temperature the sample holder was held at constant temperature, pore pressure and confining pressure for a several week period as the water and gas combined to form methane hydrate. Throughout this process the temperature, pressures and pump volumes were recorded with a standard data logging arrangement.

MRI-based data was acquired throughout the hydrate formation process with several types of images and scans. The MRI (Unity/Inova-Imaging 85/310 spectrometer, Varian Inc., Palo Alto, CA) operated at a resonance frequency of 85.7 MHz (approximately 2.0 Tesla) for hydrogen measurements. Standard 2D and 3D spin echo acquisition sequences were run with sufficient signal averaging that some of the images required up to 9 hours. The most useful information was collected as 3D images with a field of view set to 110 x 60 x 60 mm for a 128 x 32 x 32 read out and phase encoding. The resultant voxel size was 0.86 x 1.88 x 1.88 mm, which represented a sensitive volume that was comprised of several pores. The intensity in each volume therefore represented an average saturation for each cluster of hydrate-saturated pores.

Permeability was measured at several stages of the hydrate formation process by measuring the pressure drops across the core when dry nitrogen gas was flowed at several different rates through the sample assembly. The nitrogen flow tests were very short-lived, generally less than one minute, which minimized any water absorption by the gas. MRI profiles were collected during these tests to monitor dissociation of the methane hydrate. Nitrogen does not form a hydrate at the pressure and temperature conditions used in these experiments.

RESULTS

Once the core sample was placed in the holder and the fluid saturations established and stabilized the cooling system was started. It took 2 to 6 hours to reduce the sample holder temperature from room temperature, ~23^{o}C, to the desired 3.0 to 4.0^{o}C. The rate of cooling was slower during earlier experiments as system stability was tested and

evaluated. During that time the pump controlling the methane volume at constant pressure showed a slight consumption of gas (Figure 1). In this example the sharp increase in methane volume started at ~60 hours. This methane volume change corresponded to that predicted by ideal gas laws for the temperature reduction. During the same interval the MRI intensity in the core, both the whole core and core halves with spacer experiments, and in the methane-filled spacer showed a very slight increase that corresponded to these changes in density of methane.

Once the sample was cooled to the desired temperature the MRI intensity in the core remained unchanged and constant for a short period of time dependent upon the initial saturation and water salinity. After the stable period, which ranged from 2 to 24 hours, the MRI intensity in the core progressively decreased with time (Figure 1). The sharp decrease in MRI intensity in the core started at ~ 70 hours (triangles in Figure 1). This decrease corresponded to a continued consumption of methane in the experiment as noted by the increase in the methane pump volume. The MRI intensity in the spacer remained constant during the hydrate formation as no water was present in this region to form hydrate. These results illustrate how the MRI signal recognized the free water and free methane gas, when at pressure such that there was suitable molar volumes of methane. The gas contribution in the water-saturated pores, however, was relatively small and often was in the background signal. Longer 3-D acquisition sequences were needed to separate the free gas signal in the pores from the noise.

The increase in methane consumption during hydrate formation was directed towards the water-saturated pores in the core halves, and not the spacer. The decrease in MRI intensity compared favorably with the amount of methane consumed in the hydrate formation as noted by the increase in methane volume (Figure 2). The MRI intensity was inverted and normalized to signal intensity in the water-saturated core prior to cooling.
Several MRI experiments were run during the cooling and subsequent hydrate formation that provided additional insight into the process. A basic 1-D profile along the longitudinal axis of a whole core plug showed the distribution of the remaining water during the hydrate formation (Figure 3). The initial signal was collected at an initial water saturation of 1.0. The water was saturated with methane and the entire system was connected to a methane supply at constant pore pressure such that the experiment had sufficient gas to form hydrate. As the sample was cooled and hydrate formed the loss of MRI intensity along the length of the 4.5 cm core was relatively uniform. Since signal intensity is linear with water content, the loss of signal corresponded to the amount of hydrate that formed in the core. The final water saturation of 0.08 indicated that the complimentary fraction of the pore space was filled with methane hydrate. The increase in signal intensity in the spacer next to the core corresponded to the density increase in methane upon cooling. The distribution of water, and inversely the formed hydrate, remained uniform along the length of the core during the process.

The advantage of a MRI profile was the speed at which it was collected, often only minutes for suitable signal-to-noise levels. A full 3-D image required scans that took

between 1 and 9 hours to collect depending upon the desired noise levels in the core. A complete 3D image of a whole core collected during the hydrate formation process showed that the free water was evenly distributed throughout the core (Figure 4). The hydrate formation process was very efficient in this experiment with initial saturation of 0.50 and low salinity brine as all of the water (Figure 4A) was converted into hydrate (Figure 4D). The only signal that remained was the methane in the spacers at each end of the core plug. Each acquisition required 2 hours, which was short compared to the ~40 hours needed to convert the water and methane into hydrate in this experiment.

A comparison of experiments with different initial water saturations showed that hydrate formation proceeded faster when the water content was less (Figure 5). Water saturation in core plugs was set at 0.33 and 0.50 prior to cooling to hydrate formation temperatures. The brine composition was relatively dilute at 0.1 wt percent NaCl. The decrease in MRI intensity measured from the integrated volume of the core plug acquired with 3D images (for example Figure 4) monitored the extent of hydrate formation. While the lower initial water saturation formed hydrate faster, the final water saturation for the two samples was approximately the same.

A comparison of experiments with different water compositions showed that hydrate formation is affected by water activity. Experiments were run on the core-halves and spacer assembly where initial water saturation was established at 0.50. A high salinity brine of 3.0 weight percent NaCl formed hydrate at a much slower rate than the low salinity brine of 0.1 weight percent NaCl (Figure 6). In addition to the slower rate the extent of hydrate formation in the high-salinity brine was less than the low salinity brine. Hydrate formation in another experiment where brine salinity was 5.0 weight percent NaCl resulted in less than half of the original free water being converted to hydrate.

Permeability in the core was quickly reduced once hydrate formation began (Figure 7). Initial permeability in the partially water-saturated sandstone core was generally high. There was a strong correlation in permeability reduction and hydrate formation in all experiments. The final permeability was measured in the 1 to 25 mD range and was dependent upon initial water saturation and subsequent volume of hydrate formed in the pores. In no experiments did the final permeability drop below 1 mD. In several experiments the permeability was measured while the core holder was depressurized from 8.3 MPa (1200 psi) to 3.4 MPa (~500 psi) (Figure 7). The reduction in pressure caused the hydrate to dissociate as measured by the increase in MRI signal intensity. There was not a concomitant increase in permeability after the hydrate dissociation.

DISCUSSION

The advantages of using MRI images to monitor these experiments were evident from the very first. The most obvious use was that the conversion of free water and methane gas, both with strong MRI signals, to a solid hydrate phase resulted in the complete loss of detectable MRI signal as measured by conventional pulse sequences. Calibration of MRI signal intensity made it possible to estimate mass balances of hydrate and remaining free

water at a level comparable to those determined from gas volume changes. The MRI images also were crucial in establishing the initial water saturation in the core samples. The MRI images also provided a means to monitor the distribution of hydrate formation in the core plug, especially when concentrated at the ends of the core plug.

The importance of initial water saturation and brine salinity on hydrate formation was verified in these experiments. Since hydrate formation occurred at the water-gas interface, the nature of water distribution in porous media led to rapid formation relative to rates observed in bulk hydrate experiments (Natarajan et al., 1994). The abundance of fluid menisci in the partially water-saturated pores provided sufficient available surfaces for hydrate to form without creating a solid rind that poisoned subsequent growth. The pattern of hydrate growth in the core was uniform in most experiments, at least at the level detected by the MRI images. In several tests as water activity, in the molar concentration sense, decreased due to salt concentrating in the remaining water as hydrate formed there was a distinct pattern of this hydrate forming at one end of the core and then progressing along the length.
The decrease in permeability during hydrate formation was expected. What was a bit unexpected was the finite permeability that remained once most if not all of the available free water was converted to hydrate. This result was very encouraging for those interested in various production scenarios.

CONCLUSIONS

One important step in the effort to determine whether methane can be produced in commercial volumes from natural gas hydrate deposits is to run laboratory-scale experiments to test various production scenarios. The results of this study showed that hydrate formation in a porous, high permeability sandstone sample was done easily with reproducible results. The traditional indicators of hydrate formation in porous media, gas volume changes and reduction of transport properties, were complimented in this study by the use of MRI technology. The success of these hydrate formation experiments was due largely to the ability to determine the even distribution of the initial saturation in the core. The MRI images also provided direct evidence of the formation of hydrate and the patterns of formation. Hydrate formation was distributed uniformly throughout the core as measured by the sub-millimeter resolution of the MRI images. The rates and extent of hydrate formation were strongly dependent upon the initial water saturation and the salinity of the free water. Hydrate formed faster in experiments when the initial water saturation and brine salinity were lower.

REFERENCES

Baldwin, B., Moradi-Araghi, A., and Stevens, J., 2003, “Monitoring Hydrate Formation and Dissociation in Sandstone and Bulk with Magnetic Resonance Imaging”, *Magnetic Reson. Imaging,* **v. 21**, p. 1061-1069.

Buffett, B., and Zatsepina, O., 2000, “Formation of Gas Hydrates from Dissolved Gas in Natural Porous Media”, *Marine Geology,* **v. 164**, p. 69-77.

Hetland, S. and Bratteli, 2005, "A Special Core Analysis Approach to Create Gas Hydrates in Sediment Samples", Paper 29 in Proceedings International Symposium of Society of Core Analysts, August 21-25, Toronto, Canada.

Moudrakovski, I., McLaurin, G., Ratcliffe, C., and Ripmeester, J., 2004, "Methane and Carbon Dioxide Hydrate Formation in Water Droplets: Spatially Resolved Measurements from Magnetic Resonance Microimaging", *J. Phys. Chem B.*, **v. 108**, p. 17591-17595.

Natarajan, V., Bishnoi, P., and Kalogerakis, 1994, "Induction Phenomena in Gas Hydrate Nucleation", *Chem. Engin. Sci*., **v. 49**, n. 13, p. 2075-2087.

Sloan, E.D., 1998, *Clathrate Hydrates of Natural Gases, 2nd Edition*, Marcel Dekker, New York.

FIGURES

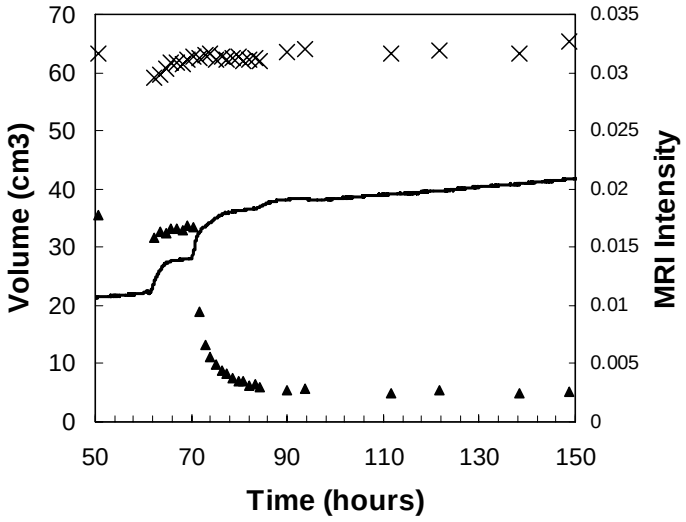

Figure 1. Composite results of hydrate formation experiment shows sharp increases in methane consumption from pump volumes (solid line), as the sample was initially cooled to 4°C (~60 hours) and when hydrate formation began (~70 hours). MRI intensity in the water-saturated core (triangles) decreased as hydrate formation began at ~70 hours. The MRI signal from methane in the spacer (X) remained constant throughout the experiment indicating a constant source of methane available to form hydrate in the core.

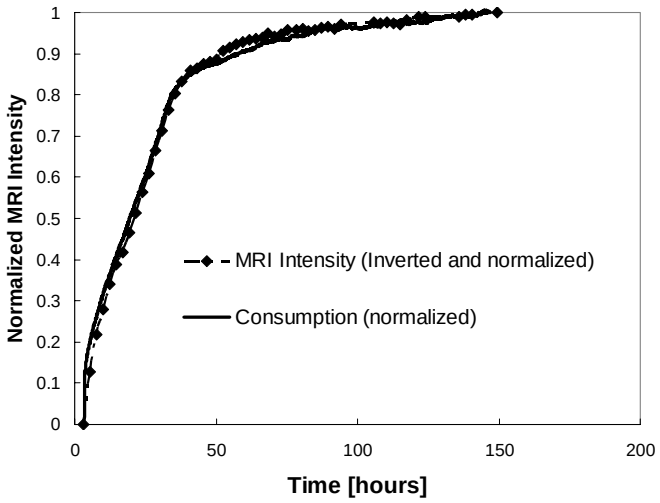

Figure 2. Comparison of MRI signal intensity and methane consumption as determined from pump volume measurements and material balance calculations for hydrate formation experiment. MRI intensity was normalized to initial water saturation, 0.50, and inverted for direct comparison of methane volumes normalized to total consumed.

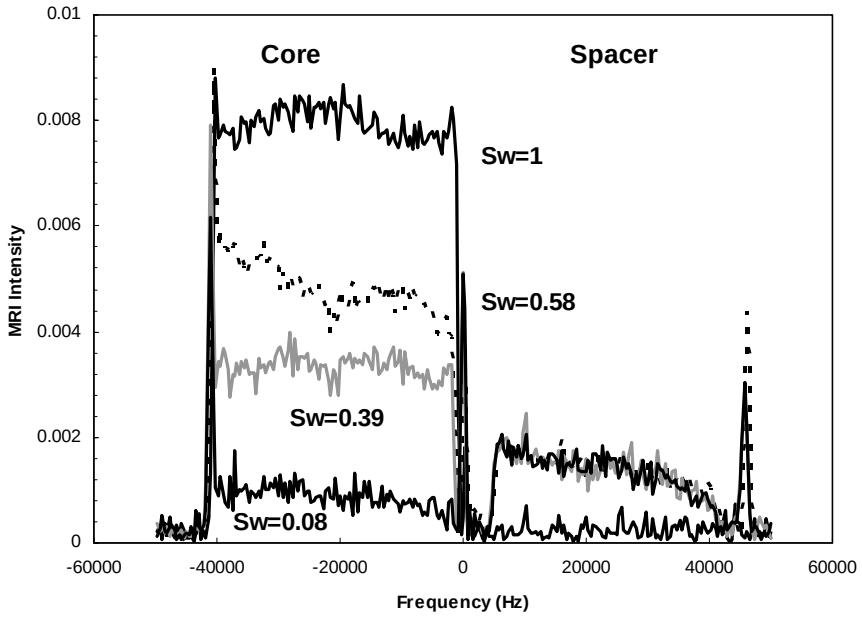

Figure 3. MRI profiles during hydrate formation in a core emphasize the uniform distribution of the remaining water throughout the process. Average water saturation at each step was estimated from MRI signal intensity. The loss of MRI signal in the core corresponds to hydrate formation. The small increase in MRI signal in the spacer corresponds to an increase in methane density due to cooling.

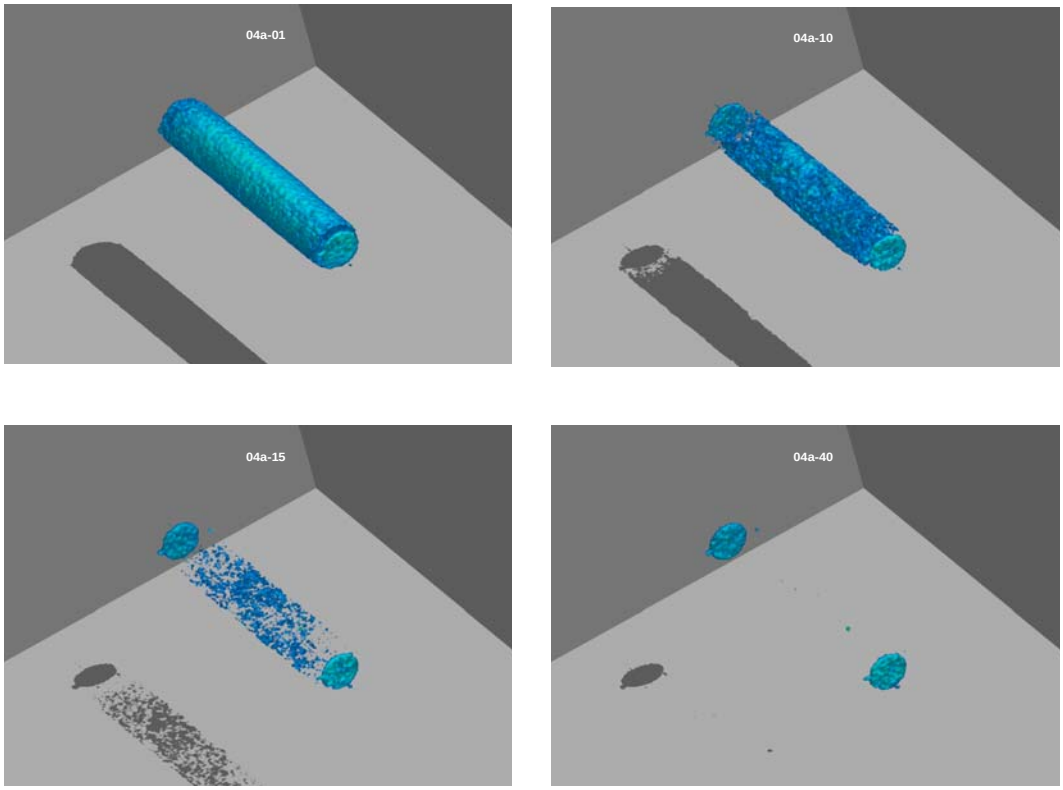

Figure 4. 3-D MRI images of water-saturated core during hydrate formation. Initial water saturation of 0.5 showed abundant signal with excess methane gas in spacers at each end (upper left). There was a progressive loss of MRI signal during hydrate formation with time (upper right- 20 hours; lower left – 32 hours) until all of the available free water was converted to hydrate (lower right – 90 hours). The remaining signal at 90 hours was methane in the end spacers. The shadow at the bottom of each image provided additional visualization of the loss of water and free methane gas signal in the core during hydrate formation.

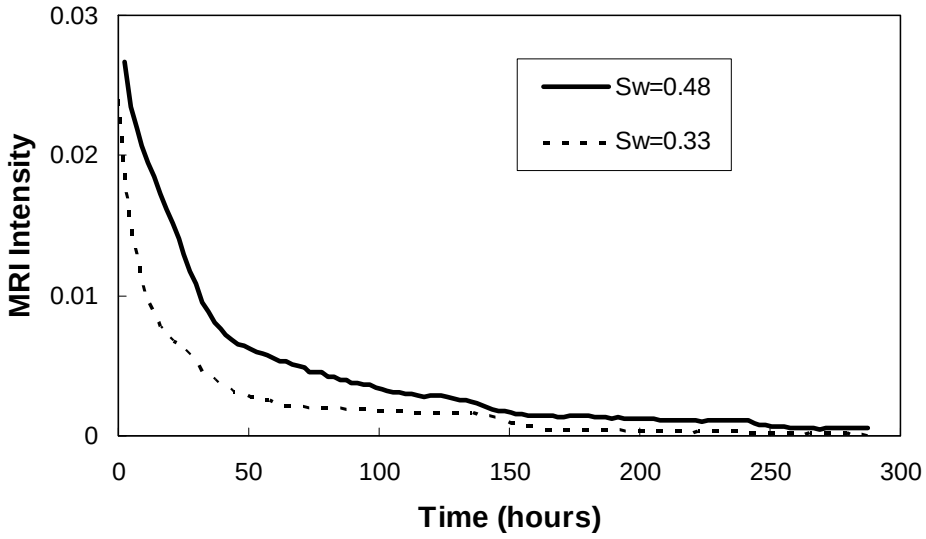

Figure 5. Hydrate formation rates and extent were illustrated by loss of MRI signal intensity for cores at initial water saturation of 0.48 (solid line) and 0.33 (dashed line). Final hydrate saturations as calculated from the loss of water content were comparable.

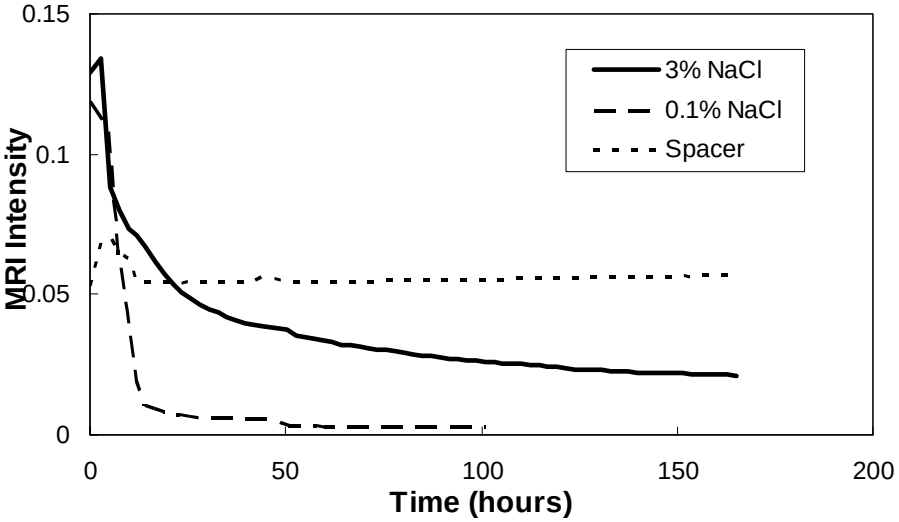

Figure 6. MRI intensity illustrated differences in hydrate formation rates as function of water salinity. The higher salinity (solid line) showed a slower formation rate than the low salinity brine (long-dashed line). MRI intensity in spacer between core halves remained constant throughout hydrate formation in the core (short-dashed line).

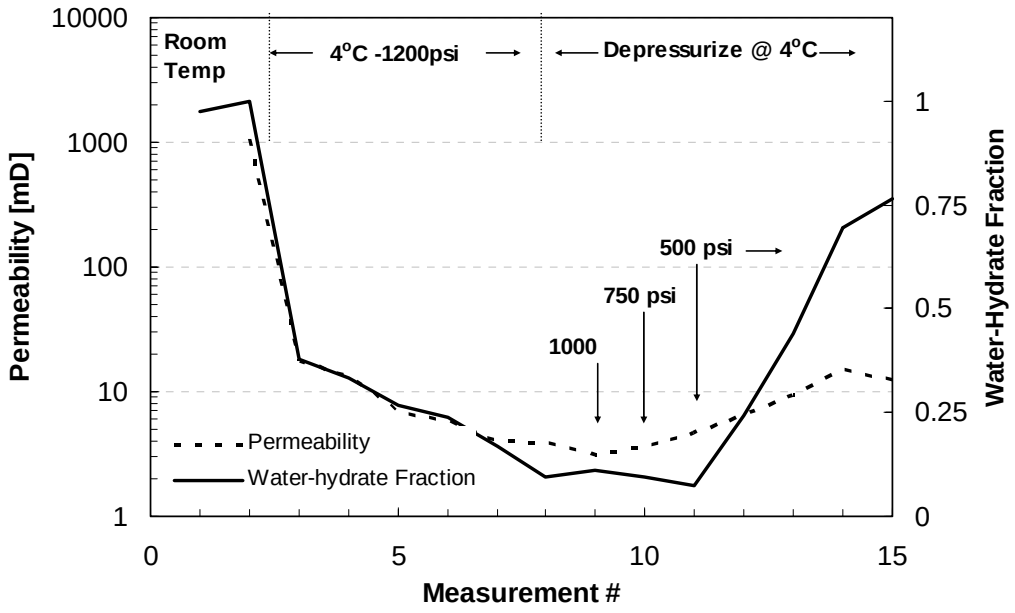

Figure 7. Reduction in permeability (dashed line) measured during hydrate formation test in a core with initial water saturation of 0.5 and water salinity of 3.0 weight percent NaCl. The loss of MRI signal intensity (solid line) began as sample was cooled from from room temperature to 4°C. Permeability reduction followed the formation of hydrate in the core. Once hydrate formation stabilized the methane gas pressure was reduced in small steps. Once below 500 psi the hydrate began to dissociate as observed by the increase in MRI signal intensity. Permeability did not show a comparable increase after the hydrate dissociated back to water and free gas.